AMERICAN ACADEMY OF OPHTHALMOLOGY®

Comparison between Spectral-Domain and Swept-Source OCT Angiography for the Measurement of Persistent Hypertransmission Defects in Age-Related Macular Degeneration

Gissel Herrera, MD,[1] Mengxi Shen, MD, PhD,[1] Omer Trivizki, MD,[1,2] Jeremy Liu, MD,[1] Yingying Shi, MD,[1] Farhan E. Hiya, MD,[1] Jianqing Li, MD,[1,3] Yuxuan Cheng, BS,[4] Jie Lu, MD, MS,[4] Qinqin Zhang, PhD,[5] Robert C. O'Brien, PhD,[1] Giovanni Gregori, PhD,[1] Ruikang K. Wang, PhD,[4,6] Philip J. Rosenfeld, MD, PhD[1]

Purpose: Spectral-domain OCT angiography (SD-OCTA) scans were tested in an algorithm developed for use with swept-source OCT angiography (SS-OCTA) scans to determine if SD-OCTA scans yielded similar results for the detection and measurement of persistent choroidal hypertransmission defects (hyperTDs).

Design: Retrospective study.

Participants: Forty pairs of scans from 32 patients with late-stage nonexudative age-related macular degeneration (AMD).

Methods: Patients underwent both SD-OCTA and SS-OCTA imaging at the same visit using the 6 × 6 mm OCTA scan patterns. Using a semiautomatic algorithm that helped with outlining the hyperTDs, 2 graders independently validated persistent hyperTDs, which are defined as having a greatest linear dimension ≥250 μm on the en face images generated using a slab extending from 64 to 400 μm beneath Bruch's membrane. The number of lesions and square root (sqrt) total area of the hyperTDs were obtained from the algorithm using each imaging method.

Main Outcome Measures: The mean sqrt area measurements and the number of hyperTDs were compared.

Results: The number of lesions and sqrt total area of the hyperTDs were highly concordant between the 2 instruments ($r_c = 0.969$ and $r_c = 0.999$, respectively). The mean number of hyperTDs was 4.3 ± 3.1 for SD-OCTA scans and 4.5 ± 3.3 for SS-OCTA scans ($P = 0.06$). The mean sqrt total area measurements were 1.16 ± 0.64 mm for the SD-OCTA scans and 1.17 ± 0.65 mm for the SS-OCTA scans ($P < 0.001$). Because of the small standard error of the differences, the mean difference between the scans was statistically significant but not clinically significant.

Conclusions: Spectral-domain OCTA scans provide similar results to SS-OCTA scans when used to obtain the number and area measurements of persistent hyperTDs through a semiautomated algorithm previously developed for SS-OCTA. This facilitates the detection of atrophy with a more widely available scan pattern and the longitudinal study of early to late-stage AMD.

Financial Disclosure(s): Proprietary or commercial disclosure may be found in the Footnotes and Disclosures at the end of this article. *Ophthalmology Science 2025;5:100593 © 2024 Published by Elsevier Inc. on behalf of the American Academy of Ophthalmology. This is an open access article under the CC BY-NC-ND license (http://creativecommons.org/licenses/by-nc-nd/4.0/).*

The clinical staging of age-related macular degeneration (AMD), including geographic atrophy (GA), which is defined as the late stage of nonexudative AMD, has been classified historically using color fundus imaging,[1,2] but, in clinical practice and clinical trials, more recent imaging modalities have been widely used to characterize the stage and progression of GA.[3,4] These other imaging methods include fundus autofluorescence, near-infrared reflectance, and OCT. As reported by the Classification of Atrophy Meeting group, OCT imaging has become the consensus imaging method for the detection of GA. When detected using OCT, GA is referred to as complete retinal pigment epithelium and outer retinal atrophy (cRORA) and defined on the basis of individual horizontal B-scans.[5] By definition, cRORA requires the presence of choroidal hypertrans mission measuring at least 250 μm along a horizontal B-scan; however, if an area of atrophy only reaches this minimum linear dimension in a nonhorizontal dimension, then this cRORA lesion would be missed. Moreover, even if an area of atrophy has a horizontal dimension

https://doi.org/10.1016/j.xops.2024.100593
ISSN 2666-9145/24

measuring at least 250 μm but the spacing between B-scans is too wide, then the region may not be detected.[6] Therefore, it would have made sense to include a minimum spacing between horizontal B-scans in the definition of cRORA.

Another OCT strategy for the detection of macular atrophy is based on locating choroidal hypertransmission defects (hyperTDs) on en face OCT imaging with dense volumetric scans of the macula.[7–18] This strategy avoids the limitations associated with the horizontal B-scans definition of cRORA. As previously described, en face OCT imaging provides a 2-dimensional view of atrophy based on images generated from slabs with boundary-specific segmentations, typically from 64 to 400 μm beneath Bruch's membrane.[9,13,19] Originally developed for use with spectral-domain OCT (SD-OCT) volume scans, this strategy has evolved to include the use of OCT angiography (OCTA) scans from either the SD-OCTA and swept-source (SS) OCTA (SS-OCTA) instruments.

Using en face imaging of dense raster SD-OCT structural scans, Shi et al[11] introduced the term persistent choroidal hyperTDs. HyperTDs identify regions that appeared bright on en face imaging due to the hypertransmission of light into the choroid at locations where the retinal pigment epithelium (RPE) is either attenuated or absent.[11] HyperTDs with a greatest linear dimension (GLD) of at least 250 μm were shown to persist over time and were therefore labeled as persistent hyperTDs.[11] Subsequently, Laiginhas et al[14] showed that these persistent hyperTDs served as precursors to the formation of typical GA.[12,14,17] Persistent hyperTDs detected on en face OCT show high overall agreement to cRORA lesions, as observed by Corvi et al,[20] but, although cRORA lesions are defined only on horizontal B-scans, persistent hyperTDs are not tied to a specific dimension. The advantages of using this en face approach for the detection of atrophy are that it can be easily and reproducibly used to detect and measure persistent hyperTDs by graders[12] and that area measurements of these hyperTDs can be easily performed, followed over time to obtain growth rate measurements, and compared with GA measurements obtained using fundus autofluorescence, near-infrared reflectance, and color imaging.[11,14,17] Moreover, using this same technique, Liu et al[17] were able to follow the formation of hyperTDs in eyes with drusen, where both the drusen area and volume could be measured simultaneously from the same scan pattern and studied as risk factors for the eventual formation of hyperTDs as the drusen measurements changed and the drusen eventually collapsed.[21] Using the same scan pattern, we have shown that other anatomic OCT biomarkers can be identified and shown to serve as predictors of disease progression such as the presence of hyperpigmentation,[16,22] basal laminar deposits,[23,24] outer retinal thinning,[8,25] and calcifying drusen.[15,26] Another advantage of using dense raster OCTA scans is the ability to detect treatment naïve nonexudative macular neovascularization, as well as the presence of exudation when it develops.[27–29]

Although SS-OCTA scans can be used to detect and measure all these anatomic biomarkers in eyes with AMD, SS-OCTA instruments are not widely available compared with SD-OCTA instruments. If en face OCTA imaging is to be widely used for the diagnosis and clinical management of eyes with AMD, it is imperative to show that the SS-OCTA algorithms are compatible with SD-OCTA scans. In this study, we used an already validated and published semi-automatic algorithm developed for the detection and measurement of hyperTDs on SS-OCTA scans and tested whether SD-OCTA scan patterns provided similar results.

Methods

Patients with AMD were enrolled in an ongoing prospective, observational, swept-source OCT and SD-OCT imaging study at the Bascom Palmer Eye Institute. The Institutional Review Board of the University of Miami Miller School of Medicine approved the study, and all patients signed an informed consent for both prospective SD-OCT and swept-source OCT studies. The study was performed in accordance with the tenets of the Declaration of Helsinki and complied with the Health Insurance Portability and Accountability Act of 1996.

A retrospective review of the prospectively enrolled subjects was performed to identify eyes with nonexudative AMD and at least 1 persistent hyperTD as manually measured on SS-OCTA and determined by 2 graders with disagreements resolved by the adjudication of a senior grader. These were eyes that had been imaged on both the SS-OCTA (PLEX Elite 9000, Carl Zeiss, Meditec Inc) and SD-OCTA (Cirrus HD-OCT 5000, Carl Zeiss, Meditec Inc) instruments using the 6 × 6 mm angiographic scan patterns centered on the fovea at the same visit.

Imaging Protocols

All the scans were acquired by 1 of 2 trained imaging technicians. The SD-OCTA instrument is powered by a superluminescent light source with a central wavelength of 840 nm and has a scan rate of 68 000 A-scans/second. The 6 × 6 mm SD-OCTA scan pattern consisted of 350 A-scans per B-scan and 350 B-scans with each B-scan repeated twice at each position, resulting in a uniform 17 μm spacing between A-scans. The SS-OCTA instrument is powered by a swept laser source with a central wavelength of 1050 nm and has a scan rate of 100 000 A-scans/second. The 6 × 6 mm SS-OCTA scan pattern consisted of 500 A-scans per B-scan and 500 B-scans with each B-scan repeated twice at each position, resulting in a uniform 12 μm spacing between A-scans. Both instruments have an optical axial resolution of approximately 5 μm in tissue and an estimated transverse resolution of approximately 15 μm at the retinal surface. Each volumetric scan was reviewed for quality and signal strength to guarantee the best quality scans to assess hyperTDs, and scans with signal strength <7 based on the instrument's output as well as scans with significant motion artifacts were excluded. In addition, eyes were also excluded if any other retinal pathologies were present, such as diabetic retinopathy, retinal vein occlusion, central serous chorioretinopathy, or if there was evidence of exudation, which was defined as the appearance of any subretinal or intraretinal fluid on structural OCT B-scans and on the retinal thickness maps.

Grading of HyperTDs

Hypertransmission defects were detected on en face structural images generated from a custom slab positioned 64 to 400 μm beneath Bruch's membrane (sub-RPE slab) for each instrument. Persistent hyperTDs were identified as areas of increased focal brightness corresponding to the hypertransmission of light into the

choroid with a GLD measuring at least 250 μm as previously reported.[11,12,14] Two independent masked graders evaluated the en face images for the presence of these lesions on both the SS-OCTA (G.H., M.S.) and SD-OCTA (G.H., O.T.) scans. HyperTDs measuring ≥250 μm in GLD were identified on the sub-RPE slabs and B-scans through the lesions were reviewed to confirm the presence of choroidal hyperTDs. Graders used a semiautomated algorithm developed by Chu et al[30] and set up a threshold tool for a GLD of ≥250 μm to generate the initial outlines of the hyperTD lesions. A built-in editing tool was used to arrive at the final outlines according to the consensus agreement of the 2 graders. Any remaining disagreement was adjudicated by a senior grader (P.J.R.). Before the area calculation using the algorithm, proper scaling factors for the SS-OCTA and SD-OCTA scans were validated. The total area measurements of the persistent hyperTDs, as well as the number of lesions and their individual areas, were provided from the algorithm output.[30,31]

Statistical Analysis

The total area of the hyperTDs was studied following the square root (sqrt) transformation strategy as previously reported.[7,8] Statistical analyses were performed using R version 4.2.2[32] with the clubSandwich[33] and tidyverse[34] packages. Linear and negative binomial regression models with cluster-robust variance estimation[35] to account for clustering of fellow eyes were used to assess the statistical significance of differences between SS-OCTA and SD-OCTA in the sqrt total area and the number of hyperTD measurements, respectively. Agreement between SS-OCTA and SD-OCTA in the sqrt total area was evaluated with Bland−Altman analysis[36] and Lin's concordance correlation coefficient (r_c).[37] A 2-sided P value < 0.05 was considered statistically significant.

Results

A total of 40 eyes from 32 patients with nonexudative AMD and evidence of macular hyperTDs were identified retrospectively for this study. These subjects underwent both SD-OCTA and SS-OCTA imaging on the same day between July 2016 to September 2022. Their ages ranged from 53 to 89 years (mean: 71.1; standard deviation [SD]: 5.8 years) and 72% were women.

The mean number of hyperTDs identified using SS-OCTA imaging was 4.5 (SD: 3.3) and 4.3 (SD: 3.1) using SD-OCTA imaging, with a lesion detection ratio of 1.053 (95% confidence interval [CI]: 0.997−1.111). This indicated that SS-OCTA scans were able to detect more hyperTDs lesions than SD-OCTA imaging, but the difference did not reach statistical significance ($P = 0.06$, Table 1). In general, not all hyperTDs detected by SS-OCTA were detected by SD-OCTA and vice versa. Of the 181 total lesions detected by SS-OCTA, there were 11 that were not detected by SD-OCTA. Of the 171 lesions detected by SD-OCTA, there was only 1 that was not detected by SS-OCTA, but most of the hyperTDs, 170 total, were detected by both scan patterns and these were in all cases the same lesions (Table 2). For SS-OCTA imaging, the mean sqrt of the total hyperTD area (SD) (Min, Max) was 1.17 (SD: 0.65) (0.26−2.49) mm and 1.16 (SD: 0.64) (0.27−2.42) mm for SD-OCTA imaging, with a mean difference of 0.014 mm (95% CI: 0.007−0.02; $P < 0.001$, Table 1, Fig. 1A). Because the small standard error of the difference between SS-OCTA and SD-OCTA of 0.003, the mean difference between the sqrt total area measurements from the 2 scan patterns was statistically significant. However, this difference was not considered to be clinically significant. Lesions detected only by SS-OCTA were smaller with a sqrt area of mean: 0.33 (SD: 0.09; minimum to maximum: 0.26−0.51) mm vs. 1.17 (SD: 0.65; minimum to maximum: 0.26−2.44) mm for lesions detected by both SS-OCTA and SD-OCTA ($P < 0.001$, Table 2). These numbers correspond to an average sqrt area per lesion of 0.21 mm for the 11 lesions detected only by SS-OCTA vs. 0.37 mm for the 170 lesions detected by both SS-OCTA and SD-OCTA. For the 1 lesion detected only by SD-OCTA, the sqrt area was 0.31 mm (i.e., an average-sized lesion; Table 2).

When comparing the sqrt total area measurements of persistent hyperTDs obtained using en face images from SD-OCTA and SS-OCTA imaging, the measurements were highly concordant ($r_c = 0.999$; Fig 1A). The Bland−Altman analysis found that the hyperTDs detected on SS-OCTA imaging had slightly larger measurements and that the differences increased with increasing hyperTD area (Fig 1B). This "proportional bias" results in limits of agreement that tend to be too wide for smaller lesions and too narrow for larger lesions.[38] However, the overall detection of hyperTDs using the 2 scan modalities resulted in similar measurements. On the other hand, when restricting the agreement analysis to only the sqrt area of the lesions shared by both SS-OCTA and SD-OCTA, we obtained a small bias (mean difference: 0.009 mm, lower LoA: −0.023, upper LoA: 0.042, and r_c: 0.9996; Table 2, Fig 1C) compared with a bias for the sqrt total area of all hyperTDs (mean difference: 0.014, lower LoA: −0.031, upper LoA: 0.058, and r_c: 0.9992; Table 1, Fig 1B). This is a quantitative affirmation of what was observed qualitatively with the lesions, i.e., there is a high degree of overlap between the lesions detected by SS-OCTA and SD-OCTA, and with few exceptions, they detect the same lesions. Figure 2 shows 2 examples with both smaller and larger lesions that result in similar hyperTDs measurements for the SS-OCTA and the SD-OCTA scans. Case #1 (Fig 2A−D) is a smaller lesion with similar sqrt total area measurements (0.61 mm for the SS-OCTA and 0.62 mm for the SD-OCTA) and the same number of hyperTD foci ($n = 2$) detected in the SS-OCTA and SD-OCTA scans. Case #2 (Fig 2E−H) is a larger size lesion with the same sqrt total area measurements (2.13 mm) and number of hyperTD foci ($n = 7$) for both scans.

Figure 3 shows examples of differences between the detection of hyperTDs on SS-OCTA and SD-OCTA images with SS-OCTA better at detecting the smaller hyperTDs compared with SD-OCTA images (Fig 3: yellow arrows). These 2 cases represent examples of smaller and larger lesions that correspond to the blue and orange asterisks in the Bland−Altman plot (Fig 1B). Case #3 (Fig 3A−D) demonstrates a smaller hyperTD (yellow arrow) that was detected in the SS-OCTA scan but missed in the SD-OCTA scan, with an overall difference between scans in the sqrt total area measurements of 0.05 mm. This case represents the smallest lesion with the largest difference

Table 1. Comparison between the Number of Persistent Choroidal HyperTDs and the Sqrt of the Total HyperTD Area Measurements Using SS-OCTA and SD-OCTA

N = 40 Eyes	SS-OCTA Mean (SD) (Minimum to Maximum)	SD-OCTA Mean (SD) (Minimum to Maximum)	Lesion Detection Ratio (95% CI)	Mean Difference (95% CI)	P Value
Number of lesions	4.5 (3.3) (1–16)	4.3 (3.1) (1–15)	1.053 (0.997–1.111)	N/A	0.06
Square root total area (mm)	1.17 (0.65) (0.26–2.49)	1.16 (0.64) (0.27–2.42)	N/A	0.014 (0.007–0.020)	<0.001

Means, standard deviations (SD), minimum, and maximum values for the number of lesions and sqrt total area of the persistent choroidal hyperTDs on SS-OCTA and SD-OCTA scans are presented above. The lesion detection ratio with its associated 95% CI for the number of lesions is equivalent to the IRR, and the *P* value shows no statistical significance; whereas for the sqrt total area of the hyperTDs, the mean diff with a 95% CI, although small, is statistically significant. For both variables, SS-OCTA measured more lesions and larger hyperTDs than SS-OCTA, but these differences were not clinically significant.
CI = confidence interval; diff = difference; hyperTDs = hypertransmission defects; IRR = incident rate ratio; Max = maximum; Min = minimum; SD = standard deviation; SD-OCTA = spectral-domain OCT angiography; sqrt = square root; SS-OCTA = swept-source OCT angiography.

found between the 2 scan types (Fig 1B, blue asterisk). Case 4 (Fig 3E–H) corresponds to an outlier with a larger lesion size (Fig 1B, orange asterisk). SS-OCTA imaging was able to detect smaller hyperTDs that were not as obvious on the SD-OCTA scan (yellow arrow). In addition, the SD-OCTA scan identified 2 larger separated hyperTDs (orange arrowhead, Fig 3G, H) that were combined in a single lesion on the SS-OCTA scan (Fig 3E, F). The overall difference in the sqrt total area measurements was 0.07 mm.

Discussion

In this study, the number and the sqrt total area of persistent hyperTDs were compared on en face images generated from sub-RPE slabs derived from 6 × 6 mm angiographic scans performed on the same day using both SD-OCTA and SS-OCTA instruments. The number and sqrt total area of the hyperTDs identified from both OCTA instruments were highly concordant with $r_c = 0.969$ and $r_c = 0.999$, respectively.

Despite the significant concordance between the 2 imaging methods, the sqrt total area of the hyperTDs showed a statistically significant mean difference ($P < 0.001$; Table 1). Furthermore, when a closer analysis of the detected lesions was performed based on the scan pattern, even the smaller mean difference (0.009) between those lesions that were detected by both modalities was statistically significant (Table 2, Fig 1C). In both cases, this was due to the small standard error of the difference in measurements, and the small mean difference was not considered to be clinically significant. The Bland–Altman plots highlight these differences showing that the measurements from SS-OCTA imaging were typically slightly larger than the ones from SD-OCTA imaging, particularly when the total area was larger (Fig 1B, C).

The mean number of persistent hyperTDs, also highly concordant ($r_c = 0.969$), showed a lesion detection ratio of 1.053 (95% CI: 0.997–1.111), indicating that SS-OCTA imaging was able to detect more hyperTD lesions than SD-OCTA imaging, although this difference was not statistically significant ($P = 0.06$, Table 1). This was further appreciated when a more detailed analysis was made to observe whether the lesions detected on SD-OCTA were the same lesions detected on SS-OCTA and the degree of

Table 2. Comparison of Persistent Choroidal HyperTD Lesions Detected by SS-OCTA and SD-OCTA

N = 40 Eyes	Number of Lesions	Sqrt Area by SS-OCTA Mean (SD) (Minimum to Maximum)	Sqrt Area by SD-OCTA Mean (SD) (Minimum to Maximum)	Mean Difference (95% CI)	P Value
Lesions detected by SS-OCTA and SD-OCTA	170	1.17 (0.65) (0.26–2.44)	1.16 (0.64) (0.27–2.42)	0.009 (0.004–0.014)	<0.001
Lesions detected by SS-OCTA but not SD-OCTA	11	0.33 (0.09) (0.26–0.51)	N/A	N/A	N/A
Lesions detected by SD-OCTA but not SS-OCTA	1	N/A	0.31	N/A	N/A

The number of all individual persistent choroidal hyperTD lesions across all 40 eyes depending on the detection by the SS-OCTA and/or SD-OCTA scans are presented above. Means, SDs, Minimum, and Maximum values for the sqrt area of the hyperTD lesions are provided for each group, i.e., lesions that were detected by both SS-OCTA and SD-OCTA vs. those detected only by SS-OCTA vs. those detected only by SD-OCTA. The mean diff of the sqrt area of the hyperTDs that were detected by both scan patterns with a 95% CI, although small, shows a statistically significant *P* value. However, these differences were not clinically significant.
CI = confidence interval; Diff = difference; hyperTDs = hypertransmission defects; Max = maximum; Min = minimum; SD = standard deviation; SD-OCTA = spectral-domain OCT angiography; sqrt = square root; SS-OCTA = swept-source OCT angiography.

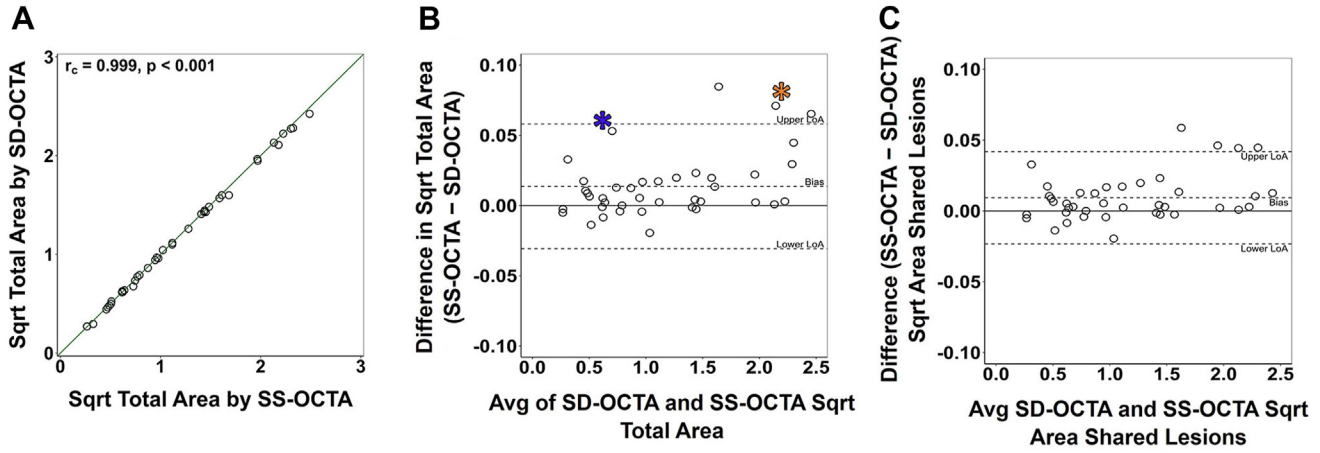

Figure 1. Concordance and Bland–Altman agreement of the square root (sqrt) total area measurements of hypertransmission defects between the spectral-domain OCT angiography (SD-OCTA) and swept-source OCT angiography (SS-OCTA) scans. **A,** The solid diagonal line represents the line of unity (slope = 1), showing the high concordance between square root area measurements of the SS-OCTA and SD-OCTA scans, with r_c = 0.999 (95% CI: 0.998–1; $P < 0.001$). **B,** The dotted line in the Bland–Altman plot represents the bias (mean difference) of 0.014 (95% CI: 0.007–0.020) with limits of agreement −0.031 (95% CI: −0.040 to −0.019) to 0.058 (95% CI: 0.037–0.075) for the estimated bias toward the slightly larger SS-OCTA measurements. Lesions with larger sqrt total area measurements tended to show a larger bias, as in the case with the orange asterisk (see also Figure 3E–H). However, at least 1 of the outliers had a smaller sqrt total area, which is represented by the case with the blue asterisk (see also Figure 3A–D). These small differences are not considered clinically significant. **C,** The dotted lines in the Bland–Altman plot represent the bias (mean difference) of 0.009 (95% CI: 0.005–0.014) with limits of agreement −0.023 (95% CI: −0.029 to −0.015) to 0.042 (95% CI: 0.028–0.053) for the lesions detected by both SS-OCTA and SD-OCTA. There was an even tighter agreement between the 2 modalities when only the shared lesions were considered. Again, these small differences are not considered clinically significant. CI = confidence interval.

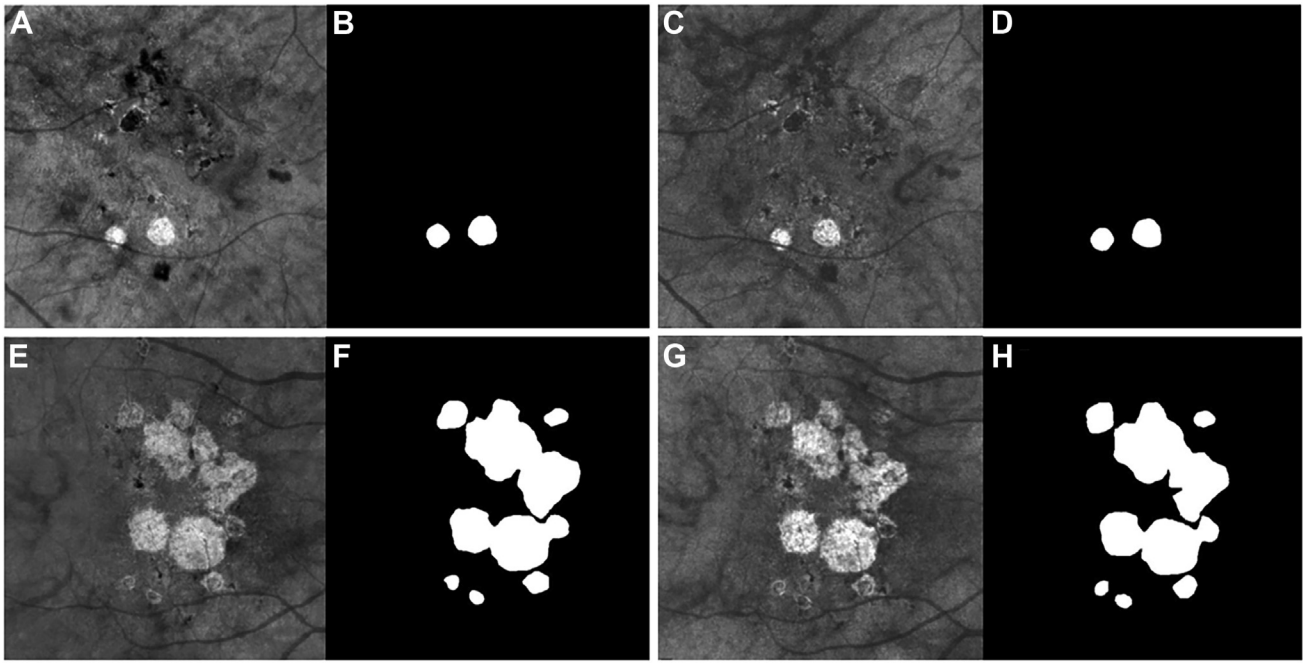

Figure 2. Similar detection and measurements of persistent hypertransmission defects (hyperTDs) with both swept-source OCT angiography (SS-OCTA) and spectral-domain OCT angiography (SD-OCTA) scans. **A–D,** An example (case 1) of a smaller size lesion, whereas **(E–H)** represent an example of a larger lesion (case 2). **A, E,** The en face SS-OCTA structural images that were created using a slab positioned 64 to 400 um under Bruch's membrane (sub-RPE slab) for the 2 cases, and **(B, F)** the corresponding outlines of each persistent hyperTD following graders consensus. **C, G,** The en face SD-OCTA structural images of the same cases in **(A, E)** using the same sub-RPE slab, and panels **D, H,** represent the corresponding hyperTDs outlines. **A, D,** Case 1 has the same number of lesions (2 hyperTDs total) and very similar square root (sqrt) total area between both scan modalities: 0.61 mm for the SS-OCTA **(A, B)** and 0.62 mm for the SD-OCTA **(C, D)** scans. **E, H,** Case 2 showed the same number of lesions despite increased multifocality (7 hyperTDs) and the same sqrt total area (2.13 mm) for both the SS-OCTA **(E, F)** and the SD-OCTA **(G, H)** scans. RPE = retinal pigment epithelium.

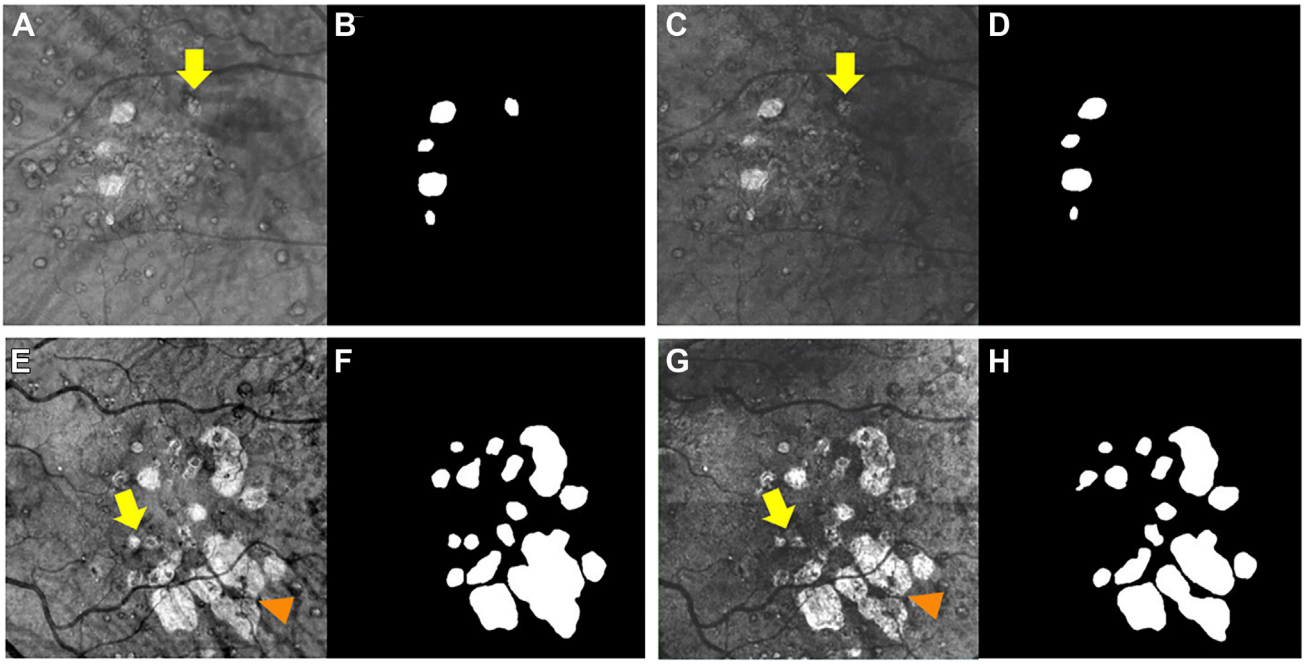

Figure 3. Differences in the detection and measurements of persistent hypertransmission defects (hyperTDs) between swept-source OCT angiography (SS-OCTA) and spectral-domain OCT angiography (SD-OCTA) scans. **A–D,** (Case 3) and (**E–H**) (case 4) represent the 2 outlier cases identified by the blue and orange asterisks respectively in the Bland–Altman plot (see Fig 1B). **A, E,** The en face SS-OCTA structural images that were created using a slab positioned 64 to 400 μm under Bruch's membrane (sub-RPE slab) for these 2 cases. **B, F,** The corresponding outlines of each persistent hyperTD following the graders' consensus. **C, G,** The en face SD-OCTA structural images of the previous 2 cases using the same sub-RPE slab, and (**D, H**) represent the corresponding hyperTDs outlines. **A–D,** Case 3, identified in the Bland–Altman plot (Fig 1B) by a blue asterisk, is the outlier with the smaller size, which showed an additional hyperTD in the SS-OCTA (**A, B**) compared with the SD-OCTA scan (**C, D**) (see yellow arrows). The square root (sqrt) total area for the SS-OCTA was 0.73 mm, and for the SD-OCTA was 0.68 mm, with a difference of 0.05 mm between both measurements. **E–H,** Case #4 (Fig 1B, orange asterisk) represents the most common type of outlier with a larger lesion size. SS-OCTA imaging (**E, F**) was able to detect smaller hyperTDs than the SD-OCTA scan (**G, H**) (see yellow arrows), and the sqrt total area was also larger: 2.18 mm for the SS-OCTA and 2.11 mm for the SD-OCTA scan, with a difference between both of 0.07 mm. Notably, 2 larger adjacent hyperTD lesions were graded as being joined together on the SS-OCTA scan (**E, F**), whereas the SD-OCTA scan was graded as having 2 separate lesions (**G, H**; see orange arrowheads). RPE = retinal pigment epithelium.

overlap between them. To this extent, we observed that most of the lesions were detected by the 2 modalities, and, with few exceptions, SS-OCTA detected more hyperTDs than SD-OCTA. These hyperTDs detected only by SS-OCTA had a much smaller sqrt area of mean and average sqrt area per lesion as compared with those shared by both scan patterns. Furthermore, only 1 hyperTD missed by the SS-OCTA was also a smaller average-sized lesion, which also happened to be part of a much larger multifocal lesion.

Then, it is possible that SS-OCTA could be somewhat better at detecting smaller hyperTDs, especially when these are part of multifocal lesions associated with an overall larger area. This ability to detect smaller foci on SS-OCTA images can be appreciated in cases 3 (panels A–D) and 4 (panels E–H) shown in Figure 3. The yellow arrows indicate some of these smaller hyperTDs that were only detected using SS-OCTA and not by SD-OCTA scans, which results in the difference in the total area measurements for these lesions. Cases 3 and 4 are also identified on the Bland–Altman plot (Fig 1B) as 2 different types of outliers in terms of total size as labeled with a blue and orange asterisk, respectively. The difference in results can be explained by the denser SS-OCTA scanning pattern, with an isotropic spacing between A-scans of 12 μm compared with 17 μm in the SD-OCTA scan, and by the longer wavelength and reduced sensitivity roll-off of the SS-OCTA instrument, which allows for better contrast and improved visualization of the smaller hyperTDs.[39] Although one could try in principle to adjust the position or thickness of the sub-RPE slab to optimize the contrast of particular hyperTDs, the current strategy using our fixed, particular choice for the sub-RPE en face slabs has been used extensively in the literature[8–12,14,17–20,25,30] and it has clear advantages. In any case, although persistent hyperTDs were initially identified on the sub-RPE en face image, each of the hyperTDs was confirmed by inspecting the corresponding B-scans for the presence of choroidal hypertransmission, the loss or attenuation of the RPE, and the loss or attenuation of the outer retina.[11,12,14]

Overall, both the SS-OCTA and SD-OCTA scans yielded similar results in the detection and measurement of persistent hyperTDs using the same semiautomated algorithm with edited manual outlines. These results are encouraging, because in the past it was not possible to use the same algorithm for the segmentation of hyperTDs on both scan modalities, given their inherent differences in the laser light,

scan pattern, and spacing, but now either SD-OCTA or SS-OCTA scans can be used for this purpose. This approach offers extra benefits to the structural and angiographical imaging of AMD because OCTA scans have a denser isotropic scan pattern than structural OCT scans and provide en face structural imaging with better image quality than typical structure-only scans. By using this method to follow eyes with AMD, we found that it is possible to identify, quantify, and follow macular atrophy and identify when exudation develops, all of which can be accomplished from a single scan pattern. This strategy would increase the efficiency of routine clinical imaging, simplify the design of clinical trials, and decrease the cost of clinical trials designed to study disease progression in nonexudative AMD.[17] Because several reports have shown the feasibility and accuracy of detecting and measuring these atrophic lesions using SD-OCT structural scans in lieu of autofluorescence imaging,[7,9–11,13,40] it is reasonable to assume that the SD-OCTA scans can be used as well. In a recent report from Baek et al,[41] a high level of agreement for the en face assessment of hyperTDs on Cirrus and Spectralis OCT was found, although, to overcome the disadvantage of the lower en face image quality of the Spectralis compared with Cirrus, they had to apply a software reconstruction of the Spectralis en face images from raw scan volume stacks, to improve the visualization of hyperTDs. Other efforts have also been performed in the past to use machine learning to segment these lesions in different OCT devices. For example, Kalra et al[42] reported good performance of models for automatic detection of hyperTDs using Spectralis OCT, which offers another layer of reassurance that hyperTDs are useful biomarkers for end points in clinical trials and can be reliably detected across different OCT devices. In any case, it is important to emphasize that although different imaging methods can certainly be used for this purpose, we do recommend the use of the same scan pattern when performing sequential measurements.

This study is subject to certain limitations, including that the current algorithm was only tested on the Zeiss Angioplex SD-OCTA scan pattern, and it is unlikely that the SD-OCTA scan pattern from another spectral-domain device will be compatible with the algorithm. Although our comparison was performed using scans from Zeiss SS-OCTA and SD-OCTA instruments, it remains to be determined if images acquired using OCTA instruments with different scan speeds and different image resolution capabilities will yield similar results. Other limitations are a constrained sample size, the selection of eyes based on the presence of at least 1 hyperTD on SS-OCTA, which can introduce a sensitivity bias toward this scan modality, and the utilization of a segmentation algorithm to initialize the manually corrected outlines. It is certainly possible that if there were >40 eyes in this study, the difference in the mean number of hyperTDs identified per eye might become statistically significant, but, based on the data we have and our choice of a 2-sided significance level of 0.05, the difference is not statistically significant and not obviously clinically significant based on the results. In the same way, we do not think that eliminating the small sensitivity bias toward the SS-OCTA scan pattern will change our results and conclusions. It could be argued that the segmentation algorithms employed in this investigation to initialize the manual outlines could possibly introduce a bias in our measurements. However, the graders very carefully reviewed and edited the outlines, and any such bias, if present, would be expected to be minimal and certainly not clinically relevant. Although congruent measurements were obtained using both SD-OCTA and SS-OCTA technologies, for the sake of longitudinal reliability, it is advisable that patients adhere to a single imaging platform, be it SD-OCTA or SS-OCTA, especially when our analysis shows a proportional bias toward the SS-OCTA measurements on larger lesions. On the other hand, the differences in quality index between the paired images could be considered to have had an effect on the hyperTD measurements, but we do not see a real impact in this regard because the graders selected only the best quality scans for the analysis and, ultimately, the measurements showed a high degree of agreement.

In summary, both SD-OCTA and SS-OCTA scans could be used to identify and measure persistent hyperTDs, finding a very strong concordance in the total area and number of identified lesions. These results suggest that either a single 6 × 6 mm SD-OCTA or SS-OCTA scan pattern can be used to perform both structural and angiographic assessment of disease progression in AMD.

Footnotes and Disclosures

Originally received: September 26, 2023.
Final revision: July 15, 2024.
Accepted: July 29, 2024.
Available online: August 7, 2024. Manuscript no. XOPS-D-23-00234R3.

[1] Department of Ophthalmology, Bascom Palmer Eye Institute, University of Miami Miller School of Medicine, Miami, Florida.

[2] Department of Ophthalmology, Tel Aviv Medical Center, Tel Aviv, Israel.

[3] Department of Ophthalmology, First Affiliated Hospital of Soochow University, Suzhou, Jiangsu, China.

[4] Department of Bioengineering, University of Washington, Seattle, Washington.

[5] Research and Development, Carl Zeiss Meditec, Inc., Dublin, California.

[6] Department of Ophthalmology, University of Washington, Seattle, Washington.

Meeting Presentation: Previously presented at the 2023 Annual Association for Research in Vision and Ophthalmology, New Orleans, LA, April 2023.

Disclosure(s):

All authors have completed and submitted the ICMJE disclosures form.

The author(s) have made the following disclosure(s):

Q.Z.: Grants or contracts from any entity − Employee of Carl Zeiss Meditec, Inc.

R.C.O.: Research support − Research to Prevent Blindness - Unrestricted Grant (GR004596-1).

G.G.: Research support − Carl Zeiss Meditec, Inc., Dublin, CA; Patents issued − along with the University of Miami, co-owns a patent that is licensed to Carl Zeiss Meditec, Inc.

R.K.W.: Research support − Carl Zeiss Meditec, Inc.; Financial support − Carl Zeiss Meditec, Inc., Colgate Palmolive Company, Estee Lauder Inc.; Consulting fees − Carl Zeiss Meditec, Inc., Cyberdontics; Honoraria − Carl Zeiss Meditec, Inc.; Patents issued − US8, 750, 586, US8, 180, 134, US9, 282,905, US9, 759,544, US10, 354,378, US10, 529,061.

P.J.R.: Research support − Carl Zeiss Meditec, Inc.; Research funding − Stealth BioTherapeutics and Gyroscope Therapeutics; Consulting fees − Abbvie, Annexon, Apellis, Bayer Pharmaceuticals, Boehringer-Ingelheim, Carl Zeiss Meditec, Chengdu Kanghong Biotech, Genentech/Roche, InflammX Therapeutics, Ocudyne, Regeneron Pharmaceuticals, Unity Biotechnology; Stock or stock options − Apellis, InflammX, Ocudyne, Valitor.

The other authors have no proprietary or commercial interest in any materials discussed in this article.

Financial Support: Research supported by grants from Carl Zeiss Meditec (Dublin, CA), the Salah Foundation, the National Eye Institute Center Core Grant (P30EY014801), and Research to Prevent Blindness (unrestricted Grant) to the Department of Ophthalmology, University of Miami Miller School of Medicine. The funding organization had no role in the design or conduct of this research.

HUMAN SUBJECTS: Human subjects were included in this study. The Institutional Review Board of the University of Miami Miller School of Medicine approved the study, and all patients signed an informed consent for both prospective spectral-domain OCT and swept-source OCT studies. The study was performed in accordance with the tenets of the Declaration of Helsinki and complied with the Health Insurance Portability and Accountability Act of 1996.

No animal subjects were used in this study.

Author Contributions:

Conception and design: Herrera, Shen, Trivizki, O'Brien, Gregori, Wang, Rosenfeld

Data collection: Herrera, Shen, Trivizki, Liu, Shi, Hiya, Li, Cheng, Lu, Zhang, Gregori, Wang, Rosenfeld

Analysis and interpretation: Herrera, Shen, Trivizki, Liu, Shi, Hiya, Li, Cheng, Lu, Zhang, O'Brien, Gregori, Wang, Rosenfeld

Obtained funding: N/A

Overall responsibility: Herrera, Shen, Trivizki, Liu, Shi, Hiya, Li, Cheng, Lu, Zhang, O'Brien, Gregori, Wang, Rosenfeld

Abbreviations and Acronyms:
AMD = age-related macular degeneration; **CI** = confidence interval; **cRORA** = complete retinal pigment epithelium and outer retinal atrophy; **GA** = geographic atrophy; **GLD** = greatest linear dimension; **HyperTD** = hypertransmission defect; **RPE** = retinal pigment epithelium; **SD** = standard deviation; **SD-OCT** = spectral-domain OCT; **SD-OCTA** = spectral-domain OCT angiography; **Sqrt** = square root; **SS-OCTA** = swept-source OCT angiography.

Keywords:
Age-related macular degeneration (AMD), En face imaging, Persistent choroidal hypertransmission defects (HyperTDs), Spectral-domain OCT angiography (SD-OCTA), Swept-source OCT angiography (SS-OCTA).

Correspondence:
Philip J. Rosenfeld, MD, PhD, Bascom Palmer Eye Institute, 900 NW 17th Street, Miami, FL 33136. E-mail: prosenfeld@miami.edu.

References

1. Ferris FLIII, Wilkinson CP, Bird A, et al. Clinical classification of age-related macular degeneration. *Ophthalmology*. 2013;120:844−851. https://doi.org/10.1016/j.ophtha.2012.10.036.
2. Fleckenstein M, Keenan TDL, Guymer RH, et al. Age-related macular degeneration. *Nat Rev Dis Primers*. 2021;7:31. https://doi.org/10.1038/s41572-021-00265-2.
3. Holz FG, Sadda SR, Staurenghi G, et al. Imaging protocols in clinical studies in advanced age-related macular degeneration: recommendations from Classification of Atrophy consensus meetings. *Ophthalmology*. 2017;124:464−478. https://doi.org/10.1016/j.ophtha.2016.12.002.
4. Jaffe GJ, Chakravarthy U, Freund KB, et al. Imaging features associated with progression to geographic atrophy in age-related macular degeneration: Classification of Atrophy Meeting Report 5. *Ophthalmol Retina*. 2021;5:855−867. https://doi.org/10.1016/j.oret.2020.12.009.
5. Sadda SR, Guymer R, Holz FG, et al. Consensus definition for atrophy associated with age-related macular degeneration on OCT: classification of Atrophy Report 3. *Ophthalmology*. 2018;125:537−548. https://doi.org/10.1016/j.ophtha.2017.09.028.
6. Wang RK, Cheng Y, Liu Z, et al. Comparison between the grading of cRORA and iRORA on SD-OCT B-scans with that of persistent hypertransmission defects on en face SS-OCT images. *Invest Ophthalmol Vis Sci*. 2023;64:327.
7. Yehoshua Z, Rosenfeld PJ, Gregori G, et al. Progression of geographic atrophy in age-related macular degeneration imaged with spectral domain optical coherence tomography. *Ophthalmology*. 2011;118:679−686. https://doi.org/10.1016/j.ophtha.2010.08.018.
8. Nunes RP, Gregori G, Yehoshua Z, et al. Predicting the progression of geographic atrophy in age-related macular degeneration with SD-OCT en face imaging of the outer retina. *Ophthalmic Surg Lasers Imaging Retina*. 2013;44:344−359. https://doi.org/10.3928/23258160-20130715-06.
9. Yehoshua Z, de Amorim Garcia Filho CA, Nunes RP, et al. Comparison of geographic atrophy growth rates using different imaging modalities in the COMPLETE study. *Ophthalmic Surg Lasers Imaging Retina*. 2015;46:413−422. https://doi.org/10.3928/23258160-20150422-03.
10. Schaal KB, Gregori G, Rosenfeld PJ. En face optical coherence tomography imaging for the detection of nascent geographic atrophy. *Am J Ophthalmol*. 2017;174:145−154. https://doi.org/10.1016/j.ajo.2016.11.002.
11. Shi Y, Yang J, Feuer W, et al. Persistent hypertransmission defects on en face OCT imaging as a stand-alone precursor for the future formation of geographic atrophy. *Ophthalmol Retina*. 2021;5:1214−1225. https://doi.org/10.1016/j.oret.2021.02.004.
12. Liu J, Laiginhas R, Corvi F, et al. Diagnosing persistent hypertransmission defects on en face OCT imaging of age-related macular degeneration. *Ophthalmol Retina*. 2022;6:387−397. https://doi.org/10.1016/j.oret.2022.01.011.
13. Velaga SB, Nittala MG, Hariri A, Sadda SR. Correlation between fundus autofluorescence and en face OCT measurements of geographic atrophy. *Ophthalmol Retina*. 2022;6:676−683. https://doi.org/10.1016/j.oret.2022.03.017.

14. Laiginhas R, Shi Y, Shen M, et al. Persistent hypertransmission defects detected on en face swept source optical computed tomography images predict the formation of geographic atrophy in age-related macular degeneration. *Am J Ophthalmol*. 2022;237:58−70. https://doi.org/10.1016/j.ajo.2021.11.001.
15. Liu J, Laiginhas R, Shen M, et al. Multimodal imaging and en face OCT detection of calcified drusen in eyes with age-related macular degeneration. *Ophthalmol Sci*. 2022;2:100162. https://doi.org/10.1016/j.xops.2022.100162.
16. Laiginhas R, Liu J, Shen M, et al. Multimodal imaging, OCT B-scan localization, and en face OCT detection of macular hyperpigmentation in eyes with intermediate age-related macular degeneration. *Ophthalmol Sci*. 2022;2:100116. https://doi.org/10.1016/j.xops.2022.100116.
17. Liu J, Shen M, Laiginhas R, et al. Onset and progression of persistent choroidal hypertransmission defects in intermediate age-related macular degeneration: a novel clinical trial endpoint. *Am J Ophthalmol*. 2023;254:11−22. https://doi.org/10.1016/j.ajo.2023.03.012.
18. Yehoshua Z, Filho CAAG, Penha FM, et al. Comparison of geographic atrophy measurements from the OCT fundus image and the sub-RPE slab image. *Ophthal Surg Lasers Imaging Retina*. 2013;44:127−132. https://doi.org/10.3928/23258160-20130313-05.
19. Shi Y, Zhang Q, Zhou H, et al. Correlations between choriocapillaris and choroidal measurements and the growth of geographic atrophy using swept source OCT imaging. *Am J Ophthalmol*. 2021;224:321−331. https://doi.org/10.1016/j.ajo.2020.12.015.
20. Corvi F, Corradetti G, Laiginhas R, et al. Comparison between B-scan and en face images for incomplete and complete retinal pigment epithelium and outer retinal atrophy. *Ophthalmol Retina*. 2023;7:999−1009. https://doi.org/10.1016/j.oret.2023.07.003.
21. Jiang X, Shen M, Wang L, et al. Validation of a novel automated algorithm to measure drusen volume and area using swept source optical coherence tomography angiography. *Transl Vis Sci Technol*. 2021;10:11. https://doi.org/10.1167/tvst.10.4.11.
22. Zhou H, Liu J, Laiginhas R, et al. Depth-resolved visualization and automated quantification of hyperreflective foci on OCT scans using optical attenuation coefficients. *Biomed Opt Express*. 2022;13:4175−4189. https://doi.org/10.1364/BOE.467623.
23. Dolz-Marco R, Balaratnasingam C, Messinger JD, et al. The border of macular atrophy in age-related macular degeneration: a clinicopathologic correlation. *Am J Ophthalmol*. 2018;193:166−177. https://doi.org/10.1016/j.ajo.2018.06.020.
24. Sura AA, Chen L, Messinger JD, et al. Measuring the contributions of basal laminar deposit and Bruch's membrane in age-related macular degeneration. *Invest Ophthalmol Vis Sci*. 2020;61:19. https://doi.org/10.1167/iovs.61.13.19.
25. Zhang Q, Shi Y, Shen M, et al. Does the outer retinal thickness around geographic atrophy represent another clinical biomarker for predicting growth? *Am J Ophthalmol*. 2022;244:79−87. https://doi.org/10.1016/j.ajo.2022.08.012.
26. Lu J, Cheng Y, Li J, et al. Automated segmentation and quantification of calcified drusen in 3D swept source OCT imaging. *Biomed Opt Express*. 2023;14:1292−1306. https://doi.org/10.1364/BOE.485999.
27. de Oliveira Dias JR, Zhang Q, Garcia JMB, et al. Natural history of subclinical neovascularization in nonexudative age-related macular degeneration using swept-source OCT angiography. *Ophthalmology*. 2018;125:255−266. https://doi.org/10.1016/j.ophtha.2017.08.030.
28. Yang J, Zhang Q, Motulsky EH, et al. Two-year risk of exudation in eyes with nonexudative age-related macular degeneration and subclinical neovascularization detected with swept source optical coherence tomography angiography. *Am J Ophthalmol*. 2019;208:1−11. https://doi.org/10.1016/j.ajo.2019.06.017.
29. Shen M, Rosenfeld PJ, Gregori G, Wang RK. Predicting the onset of exudation in treatment-naive eyes with nonexudative age-related macular degeneration. *Ophthalmol Retina*. 2022;6:1−3. https://doi.org/10.1016/j.oret.2021.10.006.
30. Chu Z, Wang L, Zhou X, et al. Automatic geographic atrophy segmentation using optical attenuation in OCT scans with deep learning. *Biomed Opt Express*. 2022;13:1328−1343. https://doi.org/10.1364/BOE.449314.
31. Chu Z, Shi Y, Zhou X, et al. Optical coherence tomography measurements of the retinal pigment epithelium to Bruch membrane thickness around geographic atrophy correlate with growth. *Am J Ophthalmol*. 2022;236:249−260. https://doi.org/10.1016/j.ajo.2021.10.032.
32. Version. *R: A language and environment for statistical computing*. R Foundation for Statistical Computing; 2023. https://www.R-project.org/. Accessed June 7, 2023.
33. Cluster-Robust (Sandwich) Variance Estimators with Small-Sample Corrections. *Version R package version 0.5.8. cran.r-project.org*; 2022. http://jepusto.github.io/clubSandwich/. Accessed June 7, 2023.
34. Wickham H, Averick M, Bryan J, et al. Welcome to the Tidyverse. *J Open Source Softw*. 2019;4:1686. https://doi.org/10.21105/joss.01686.
35. Pustejovsky JE, Tipton E. Small-sample methods for cluster-robust variance estimation and hypothesis testing in fixed effects models. *J Bus Econ Stat*. 2018;36:672−683. https://doi.org/10.1080/07350015.2016.1247004.
36. Bland JM, Altman DG. Statistical methods for assessing agreement between two methods of clinical measurement. *Lancet*. 1986;1:307−310.
37. Lin LI. A concordance correlation coefficient to evaluate reproducibility. *Biometrics*. 1989;45:255−268.
38. Bland JM, Altman DG. Measuring agreement in method comparison studies. *Stat Methods Med Res*. 1999;8:135−160. https://doi.org/10.1177/096228029900800204.
39. Miller AR, Roisman L, Zhang Q, et al. Comparison between spectral-domain and swept-source optical coherence tomography angiographic imaging of choroidal neovascularization. *Invest Ophthalmol Vis Sci*. 2017;58:1499−1505. https://doi.org/10.1167/iovs.16-20969.
40. Schaal KB, Rosenfeld PJ, Gregori G, et al. Anatomic clinical trial endpoints for nonexudative age-related macular degeneration. *Ophthalmology*. 2016;123:1060−1079. https://doi.org/10.1016/j.ophtha.2016.01.034.
41. Baek J, Ashrafkhorasani M, Mahmoudi A, et al. En face and volumetric comparison of hypertransmission defects evaluated by Cirrus and Spectralis optical coherence tomography. *Am J Ophthalmol*. 2024;264:135−144. https://doi.org/10.1016/j.ajo.2024.03.003.
42. Kalra G, Cetin H, Whitney J, et al. Machine learning-based automated detection and quantification of geographic atrophy and hypertransmission defects using spectral domain optical coherence tomography. *J Pers Med*. 2022;13:37. https://doi.org/10.3390/jpm13010037.